THE JOURNAL OF PHYSICAL CHEMISTRY C

Article

pubs.acs.org/JPCC

One-Step Synthesis of Au−Pd Alloy Nanodendrites and Their Catalytic Activity

Lihua Shi,[†,‡] Aiqin Wang,[†] Tao Zhang,*[,†] Bingsen Zhang,[§] Dangsheng Su,[§] Huanqiao Li,[∥] and Yujiang Song[∥]

[†]State Key Laboratory of Catalysis, Dalian Institute of Chemical Physics, Chinese Academy of Sciences, Dalian 116023, P. R. China

[‡]University of Chinese Academy of Sciences, Beijing, 100049, P. R. China

[§]Catalysis and Materials Division, Shenyang National Laboratory for Materials Science, Institute of Metal Research, Chinese Academy of Sciences, Shenyang 110016, P. R. China

[∥]Dalian National Laboratory for Clean Energy, Dalian Institute of Chemical Physics, Chinese Academy of Sciences, Dalian 116023, P. R. China

Supporting Information

ABSTRACT: Au−Pd bimetallic nanocrystals with well-defined dendritic morphology, uniform size, and homogeneous alloy structure were synthesized in an aqueous solution by using ascorbic acid as the reductant and triblock copolymer P123 as the stabilizing agent. In this synthesis, ascorbic acid played a key role in directing the nanodendritic morphology while the presence of Pd was mandatory for the formation of well-defined nanodendrites. Without Pd, only faceted nanoparticles of gold were formed under the same reaction conditions. Other reaction variables such as the addition sequence and the dropping rate of the metal precursors, the type and concentration of the stabilizing agents, and the reaction time and temperature were all found to affect the size uniformity and morphology perfectness to some extent. The Au/Pd atomic ratio could be tuned in a wide range without deteriorating the nanodendritic morphology. The as-prepared Au−Pd nanodendrites exhibited excellent catalytic activities toward electroxidation of methanol and reduction of 2-nitrophenol, and the catalytic performances could be effectively tuned by the Au/Pd ratio.

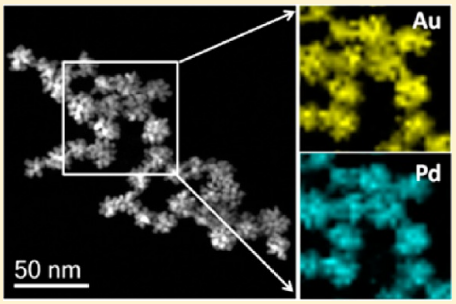

INTRODUCTION

Heterogeneous catalysis with nanocrystals (NCs) is critically dependent on the size and shape. While size effect has been well established,[1−5] the effect of shape or morphology of NCs on the catalytic performance is still far less understood due to the difficulties in morphology control of NCs, especially within a range of catalytically active sizes (<10 nm).[6−9] In the past decade, there has been an intensive research interest in the synthesis of NCs with various morphologies and solution-based method which involves the reduction of metal precursors in the presence of structure-directing agent or stabilizing agents has shown great potentials in the shape control of NCs.[6−16] Among various morphologies such as nanowires,[10,11] nanocubes,[9,10,12] multipods,[14] etc., nanodendrites are a kind of intriguing catalytic material owing to their porous structures, large surface areas, and in particular small sizes of each individual branch in the dendrites (<10 nm) which are required for a good catalyst.[15−23] The formation of a nanodendritic structure is usually thought as a consequence of a slow nucleation followed by fast growth which can be manipulated by varying reducing agent and reaction conditions.[15,16,21−27] Although nanodendritic noble metals including Pt, Pd, Au, Rh, etc., have been synthesized via the solution method,[15−28] the synthesis of bimetallic nanodendrites with both shape and chemical composition in a controllable manner is still a challenge, in particular with a homogeneous alloy structure.

Bimetallic NCs often exhibit superior catalytic performances than the monometallic counterparts due to synergistic effect between two different metals and great tunability in chemical compositions and structures.[18−23,29−34] Among different bimetallic systems, AuPd bimetallic NCs have received great interest as they can be widely used as effective catalysts for various reactions, such as selective oxidation of alcohols,[35−38] direct synthesis of H_2O_2 from H_2 and O_2,[39−41] N_2O decomposition,[42] Suzuki−Miyaura and Heck coupling reactions,[43] and electrochemical reaction.[44,45] The great potential of Au−Pd bimetallic catalysts has prompted morphology-controlled synthesis of Au−Pd NCs. For example, Huang and coworkers used Au nanocubes as structure-directing core to prepare tetrahexahedral Au−Pd core−shell nanocrystals with high-index {730} planes, and the obtained Au−Pd tetrahexahedral nanocrystals exhibited much higher electrocatalytic activity than that of {111}-facet-bounded octahedral nanocrystals.[44] Also using a seeded synthesis approach, Xu et al. prepared

Received: February 5, 2013
Revised: May 29, 2013
Published: May 30, 2013

   dx.doi.org/10.1021/jp4013202 | J. Phys. Chem. C 2013, 117, 12526−12536

nanoflowers with a Au core and Pd petals through the reduction of $PdCl_4^{2-}$ ions by hydroquinone in the presence of gold nanoparticles and PVP, and they ascribed the formation of nanoflower morphology to the attachment of homogeneously nucleated Pd clusters to gold seed.[46] Alternatively, Au−Pd bimetallic NCs can be synthesized by coreduction of two metal precursors without the presence of seed, and the resultant NCs can be core−shell structure or homogeneous alloy depending on the reducing agent and reaction conditions. For instance, Han et al. reported the synthesis of flower-like Au−Pd bimetallic NCs through sodium citrate coreduction of Au and Pd ions.[47] The higher capability of citrate to reduce Au ions than Pd ions resulted in the Au-rich core and Pd-rich shell structures. In order to obtain flower-like Au−Pd NCs with a homogeneous alloy structure, Lee et al. used ascorbic acid as the reducing agent to accomplish the coreduction of $HAuCl_4$ and K_2PdCl_4. Nevertheless, cyclic voltammetry measurements indicated their Au−Pd alloy NCs had Pd-enriched surfaces.[48] In a following work, they used a stronger reducing agent, hydrazine hydrate ($N_2H_4{\cdot}H_2O$), to accelerate the homogeneous nucleation of Au and Pd and obtained homogeneous alloy structure with nanodendritic morphology.[49] By integration of seed-mediated synthetic method and coreduction method, Desantis et al. succeeded in manipulating the growth kinetics and prepared Au/Pd octopods and concave core@shell Au@Pd NCs using ascorbic acid as the reducing agent and cetyltrimethylammonium bromide (CTAB) as the stabilizing agent.[50,51]

From the above work one can see that the morphology of NCs is strongly dependent on the type of reducing agent. Although Au−Pd alloy NCs with dendritic morphology could be synthesized by using hydrazine as the reducing agent, neither morphology nor size was uniform possibly because the nucleation rate was too fast to be controlled very well. Furthermore, hydrazine is highly toxic and unsuitable for large-scale application. Therefore, it is highly desirable to use a cheap and nontoxic reducing agent for the synthesis of Au−Pd nanodendrites with uniform sizes and homogeneous alloy structure. Previous work has demonstrated that ascorbic acid was a very effective reducing agent in the synthesis of Pt or Pt-based multicomponent dendritic structures,[21−26] but it failed to produce Au and Pd nanodendrites under identical reaction conditions.[21,22,26] The formation of Pt nanodendrites was tentatively attributed to the strong affinity between block copolymer and Pt.[21,22,25,26]

In the present work, we report successful synthesis of Au−Pd nanodendrites with uniform sizes of about 20 nm and well-defined dendritic morphology. The distinctive feature of our synthesis strategy from those reported earlier lies in that the precursor solution of Au and Pd ions was added dropwise to the ascorbic acid solution in the presence of Pluronic P123. The slow addition procedure allows one to manipulate well the nucleation and growth rates of NCs for the formation of well-defined nanodendrites with homogeneous alloy Au−Pd nanostructures. More importantly, each individual branch in the nanodendrites has very small sizes (3−5 nm), and tens of these branches constitute a very open and easily accessible nanodendritic structure which will be favorable to catalysis. The synthesis variables were investigated in detail, among which both the ascorbic acid and the Pd component were found to play a key role in directing the nanodendritic morphology. Finally, the resultant Au−Pd alloy nanodendrites were evaluated for the electrocatalytic oxidation of methanol and the reduction of 2-nitrophenol, and they exhibited promising and tunable activities depending on the Au/Pd ratio.

EXPERIMENTAL SECTION

Synthesis of Au−Pd Bimetallic Nanodendrites. The Au−Pd bimetallic nanodendrites were synthesized by coreduction of $HAuCl_4$ and H_2PdCl_4 with ascorbic acid in the presence of stabilizing agent Pluronic P123, using a special dropping addition procedure. Typically, 5.0 mL of an aqueous solution containing 50.6 mg of Pluronic P123 and 88.0 mg of ascorbic acid was added into a 15 mL vial and mixed uniformly under continuous stirring at 25 °C. Subsequently, 5.0 mL of an aqueous solution containing 6.25 μmol of $HAuCl_4$ and 6.25 μmol of H_2PdCl_4 was added into the vial at a constant flow rate of 0.22 mL/min by a peristaltic pump. The total concentration of the metal precursors in the final reaction solution was 1.25 mM with varied Au/Pd ratios, and the molar ratio in the synthesis recipe was metal ion/ascorbic acid/P123/H_2O = 1/40/0.7/44800. After addition, the mixture was kept stirring at 25 °C for another 1 h to yield a dark brown solution. The obtained Au−Pd bimetallic nanodendrites were collected by centrifugation at 10 000 rpm for 20 min and washed three times with ultrapure water. Then the product was redispersed into water for further use.

Characterization. Transmission electron microscopy (TEM) was conducted with a JEOL 2000EX electron microscope operating at 200 kV and a Tecnai G^2 Spirit FEI transmission electron microscope operating at 120 kV. High-resolution TEM (HRTEM) and high angle annular dark field (HAADF) images were obtained on an FEI Tecnai G^2 F30S-Twin microscope operating at 300 kV. Before TEM examination, the samples were ultrasonically dispersed in water, and several drops were put onto 230 mesh copper grids coated with an ultrathin carbon film. X-ray powder diffraction (XRD) patterns were recorded with a PW3040/60 X'Pert PRO (PANalytical) diffractometer operating at 40 kV and 40 mA by using a Cu Kα radiation source. The chemical compositions of the nanodendrites were determined by energy-dispersive X-ray spectroscopy (EDS) attached on TEM and by inductively coupled plasma (ICP) spectrometer on an IRIS Intrepid II XSP instrument. X-ray photoelectron spectroscopy (XPS) was performed on the VG ESCALAB MK2 instrument using Al Kα radiation (1486.6 eV, 12.5 kV, 250 W). Before fitting, a Shirley background was subtracted, and the contamination of the alloy was corrected through the C 1s line (284.6 eV). The surface relative atomic concentration was calculated using the approximate formula[52] $n_i/n_j = I_i/I_j \times \sigma_j/\sigma_i \times Ek_j^{0.5}/Ek_i^{0.5}$, where n represents the number of surface atoms, I represents the peak intensity of XPS and can be calculated by peak area, and σ represents the ionization cross section of the corresponding energy level and can be calculated by Scofield.[53] Since the binding energy of Pd $3d_{5/2}$ overlapped with that of Au $4d_{5/2}$, the contribution of Au $4d_{5/2}$ was subtracted from the Pd 3d spectrum by curve-fitting. Then the surface atomic concentrations of Au and Pd were calculated by Au $4f_{5/2}$ and Pd $3d_{3/2}$, respectively.

Electrocatalytic Measurements. The electrochemical measurements were carried out in a standard three-electrode cell on a CHI 760 electrochemical workstation. The counter electrode is a Pt mesh (1 cm × 1 cm), the reference electrode is an Hg/Hg_2SO_4 electrode, and the working electrode is a glassy carbon rotating disk electrode. To prepare the working electrode, the sample of Au−Pd nanodendrites was ultrasoni-

dx.doi.org/10.1021/jp4013202 | J. Phys. Chem. C 2013, 117, 12526−12536

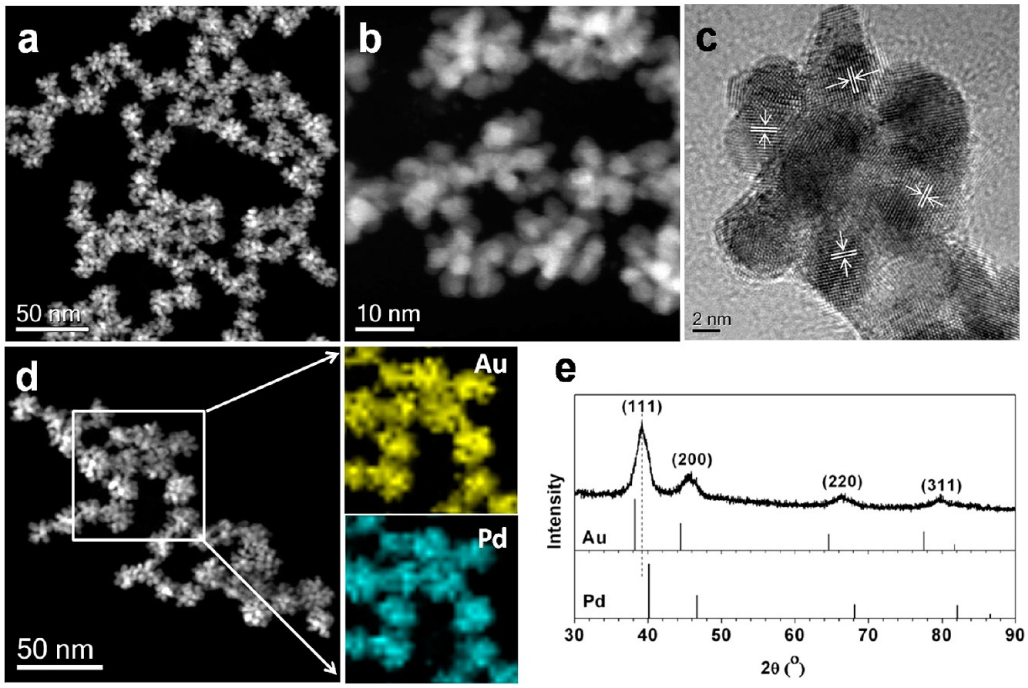

Figure 1. (a–c) HAADF-STEM, high-magnification HAADF-STEM, and HRTEM images, (d) HAADF-STEM-EDS mapping images, and (e) XRD patterns of Au/Pd = 1/1 nanodendrites. The sample was synthesized with the following reactant concentrations: 1.25 mM ($HAuCl_4$ + H_2PdCl_4), 0.1 M ascorbic acid, 5.06 g/L P123. The dropping rate was 0.22 mL/min.

cally dispersed in water to form a homogeneous solution, and then a certain amount of the solution was put onto the glassy carbon disk. After drying, 10 μL of a 0.025% Nafion solution was added onto the working electrode. The metal loading for all samples was 50 $\mu g/cm^2$. Cyclic voltammetry (CV) was conducted in a N_2-saturated 0.1 M KOH solution at a scan rate of 20 mV/s. For methanol oxidation, CVs were achieved in a N_2-saturated 0.1 M KOH and 0.5 M methanol solution at a scan rate of 50 mV/s. All the experiments were performed at 25 °C.

Catalytic Reduction of 2-Nitrophenol. In a typical reaction, 1 mL of 0.2 mM aqueous solutions of 2-nitrophenol was mixed with 0.5 mL of 15 mM $NaBH_4$ aqueous solution, and then 1 mL of ultrapure water was added into the mixture. Before the addition of the Au–Pd catalyst, the sample of Au–Pd nanodendrites was ultrasonically dispersed in water to form a homogeneous solution, and then a certain amount of the solution was added into the mixed 2-nitrophenol solution with the catalyst/substrate ratio of 1/30. As the reaction proceeded, the reaction solution changed from yellow to colorless, and the reaction progress was monitored with the UV–vis spectrometer. The intensity of the absorption peak at 415 nm in the UV–vis spectrum was used as an indicator of the reduction.

RESULTS AND DISCUSSION

Morphology of Nanocrystals. The typical procedure for the synthesis of Au–Pd bimetallic nanodendrites is illustrated in Scheme S1, in which the mixture solution of Au and Pd precursors was added slowly with a peristaltic pump into the solution containing Pluronic P123 and ascorbic acid. The excess amount of reducing agent ensures simultaneous reduction of Au and Pd cations, favoring the formation of Au–Pd alloy phase. Figure 1 shows the HRTEM, HAADF-STEM, and elemental mapping images as well as XRD patterns of the NCs obtained with this procedure. It can be clearly seen that the NCs are uniformly dispersed and well-defined nanodendrites, having an average size of ~20 nm. Each individual nanodendrite is composed of 7–9 branches, and the size of each branch is 3–5 nm (Figure 1b,c). Such an open nanodendritic structure and small primary particle sizes are expected to find interesting applications in catalysis.[18,19,22] From the HRTEM image in Figure 1c, one can observe the lattice fringes of these branch particle are in various orientations, indicating the nanodendrites are of polycrystalline structure. This is quite different from those of Pt-group metal nanodendrites derived from the reduction of ascorbic acid where single crystalline structure was always formed.[24,25] The lattice distance of each primary particle is 2.30 Å, which is well consistent with the (111) planes of Au–Pd alloy,[47] indicating the formation of Au–Pd alloy phase. To further confirm the alloy structure of AuPd nanodendrites, HAADF-STEM-EDS analysis was performed. As shown in Figure 1d, the distribution of Au atoms is completely consistent with that of Pd atoms, confirming the formation of homogeneous Au–Pd alloy nanostructures, rather than core–shell structures.

Figure 1e shows the XRD pattern of the Au–Pd nanodendrites. Four reflections appear at 39.2°, 45.6°, 66.4°, and 79.8°, which are coincidently located between Au (reference code: 00-004-0784) and Pd (reference code: 00-005-0681) and can be indexed as the (111), (200), (220), and (311) reflections of the face-centered cubic AuPd alloy. By applying Vegard's law to the above XRD pattern, the chemical composition of Au–Pd nanodendrites can be estimated to be $Au_{49}Pd_{51}$, which agrees well with the Au/Pd = 1/1 in the reaction mixture, thus further corroborating the formation of uniform Au–Pd alloy. According to Scherrer formula, the crystalline size of Au–Pd nanodendrites was calculated to be 4.7 nm, which is well accordant with the size of each branch particle (~5 nm) in TEM images.

dx.doi.org/10.1021/jp4013202 | J. Phys. Chem. C 2013, 117, 12526–12536

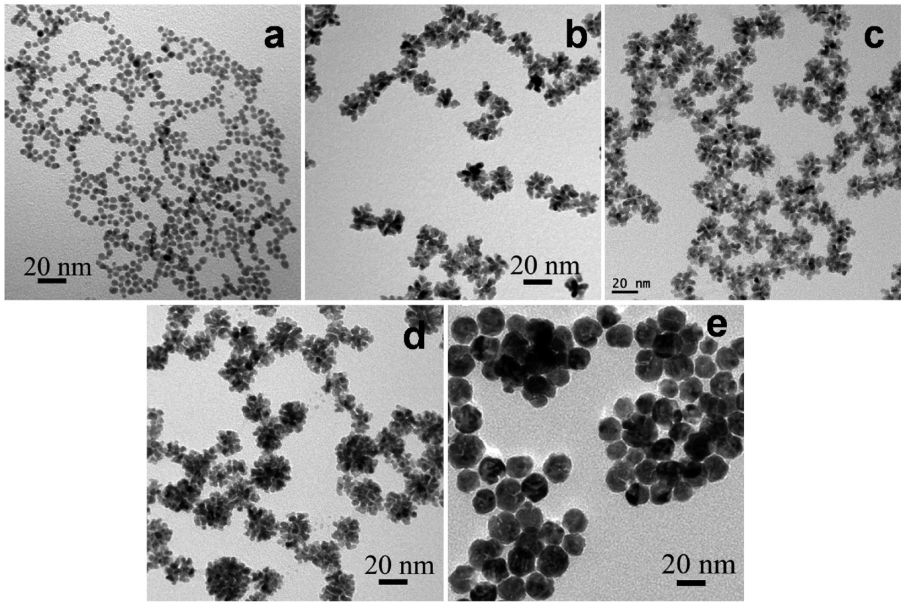

Figure 2. TEM images of Au−Pd nanostructures synthesized with different addition rate of Au and Pd precursors solution and different addition sequence. (a) Au and Pd precursors solution was poured into the reaction system. (b−d) Au and Pd precursors solution was added dropwise at a rate of (b) 0.04, (c) 0.22, and (d) 0.63 mL/min. (e) Ascorbic acid was dropped into the mixture solution of Au and Pd precursors and P123 at a rate of 0.22 mL/min.

It should be mentioned that both the yield (nearly 100%) and the quality of the nanodendrites did not decrease even when the total concentration of two metal precursors was increased from 5 to 20 mM (Figure S1), demonstrating the high efficiency of this synthesis method in producing well-defined and uniform Au−Pd bimetallic nanodendrites.

Effect of Addition Sequence. The morphology of NCs is highly dependent on the nucleation and growth kinetics, which can be manipulated by tailoring the reaction parameters. First, it was found that the addition sequence and rate of the precursor solution affected significantly the morphology of the resultant NCs. As shown in Figure 2a, when the precursor solution of Au and Pd was quickly poured into the solution of P123 and ascorbic acid, nearly spherical Au−Pd NCs with an average diameter of 4.7 nm were produced. This spherical morphology is expected considering that the pouring addition results in instantaneous production of a vast amount of nuclei, meanwhile restraining nuclei growth by exhausting of metal precursors and thus favoring the formation of small spherical particles.[54,55] In contrast, as the precursors were added dropwise, the concentrations of Au and Pd atoms were relatively low, which resulted in well-controlled nucleation and growth rate. In this case, both the heterogeneous and homogeneous nucleation may take place concurrently. For the heterogeneous nucleation, the initially formed particles act as the seeds to direct the formation of dendritic morphology with a continuous dropwise addition of the precursors. On the other hand, for the homogeneous nucleation, the formation of nanodendrites is a consequence of attachment of primary particles under the presence of shape-directing agent. In the following discussion of the morphology evolution, we will demonstrate that the constant dropping addition is favorable to the homogeneous nucleation followed by oriented attachment of initially formed particles. The nanodendrites could be produced in a wide range of dropping rate, from 0.04 to 0.63 mL/min, but the sizes and morphology uniformity were slightly varied (Figure 2b−d). In our investigated conditions, the dropping rate of 0.22 mL/min was found to be most suitable for yielding uniform and well-defined nanodendrites. In addition, if we adopted an inverse dropping procedure, i.e., the reducing agent ascorbic acid was dropped slowly into the mixture solution containing P123 and metal precursors, irregular shaped particles with an average size of ∼20 nm were obtained (Figure 2e). UV−vis spectra (not shown here) indicated the formation of separate gold nanoparticles instead of Au−Pd alloy structure, which is due to the insufficient amount of reducing agent in the reaction mixture and the higher standard reduction potential of $HAuCl_4$ than H_2PdCl_4 ($AuCl_4^-$/Au, 1.002 V; $PdCl_4^{2-}$/Pd, 0.591 V).[47] Therefore, when one uses a weak reducing agent to produce homogeneous Au−Pd alloy structure while maintaining a dendritic morphology, dropping addition of metal precursors to the solution of reducing agent is necessary to guarantee the simultaneous reduction of Au and Pd cations and a well-controlled nucleation and growth rate.

Effect of Reducing Agent. In the formation of Au−Pd alloy nanodendrites, the employment of ascorbic acid as the reducing agent was found to be critical. To demonstrate the key role of ascorbic acid, we compared different reducing agents: sodium borohydride ($NaBH_4$) which is stronger than ascorbic acid in reducing power and formic acid (HCOOH) which is weaker than ascorbic acid. Figure 3 shows the representative TEM images of Au−Pd NCs synthesized by using different reducing agents while keeping the other parameters identical. Unlike the well-defined nanodendrites obtained by using ascorbic acid, $NaBH_4$ induced the formation of nanowire networks of Au−Pd alloy (Figure 3a). In our previous work, we also obtained the similar nanowire morphology of Au−Cu alloy by the employment of $NaBH_4$.[11] In contrast, when HCOOH was used as the reducing agent, very large (∼20 nm) and irregular-shaped NCs were produced (Figure 3b). The differences in the morphology of NCs can be attributed to the disparity of reaction kinetics caused by the reducing ability. The strong reducing power of $NaBH_4$ made the Au−Pd nuclei

dx.doi.org/10.1021/jp4013202 | J. Phys. Chem. C 2013, 117, 12526−12536

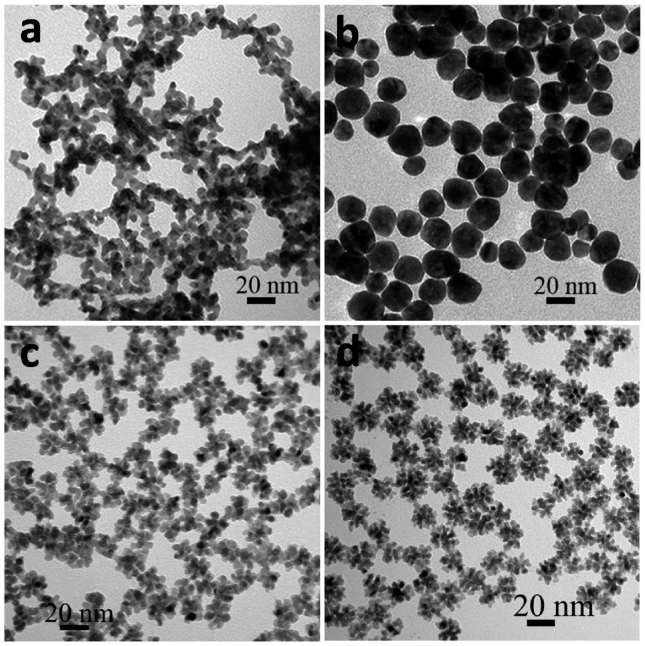

Figure 3. TEM images of Au–Pd nanostructures synthesized with different reductant (a) 0.1 M $NaBH_4$, (b) 0.1 M HCOOH, (c) 0.01 M ascorbic acid, and (d) 0.2 M ascorbic acid.

burst out instantaneously and grow into the nanowire networks quickly, driven by minimizing the surface energy of nuclei.[11] However, due to the weak reducing ability of HCOOH, only $HAuCl_4$ was reduced while H_2PdCl_4 could not be reduced, which resulted in the formation of irregular-shaped and very large gold particles. To confirm this point, we measured the UV–vis spectra of different species produced respectively by reduction of ascorbic acid and HCOOH. As shown in Figure 4,

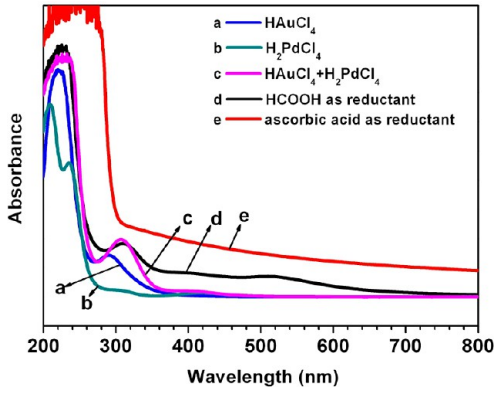

Figure 4. UV–vis spectra of precursor solutions and nanocrystals produced by reduction with different reducing agents.

the precursor mixture of $HAuCl_4$ and H_2PdCl_4 presented two broad absorption peaks at 225 and 308 nm (curve c), which can be deconvoluted into two absorption peaks of $HAuCl_4$ at 226 and 290 nm (curve a) and three absorption peaks of H_2PdCl_4 at 208, 235, and 310 nm (curve b). Upon reduction by HCOOH (curve d), the absorption peaks of $HAuCl_4$ disappeared completely, and a new peak appeared concurrently at 520 nm which is characteristic of gold nanoparticles.[42] Meanwhile, the absorption peaks of H_2PdCl_4 remained unchanged, indicating $HAuCl_4$ was reduced to Au particles while H_2PdCl_4 was not. In contrast, when ascorbic acid was used as the reducing agent (curve e), the absorption peaks of both Au and Pd precursors vanished completely, and no any new peak was yielded, indicating the formation of Au–Pd alloy nanostructures.[42] Evidently, ascorbic acid is the most suitable reducing agent for the formation of dendritic Au–Pd alloy nanostructures. It should be pointed out that in a wide range of concentration of ascorbic acid, from 0.01 to 0.2 M (Figure 3c,d), well-defined and monodispersed nanodendrites were always produced. It was proposed that ascorbic acid not only acted as a reducing agent but also served as a shape-directing agent in the synthesis of hyperbranched Pt nanostructures due to the binding ability of DGA (a byproduct derived from ascorbic acid during reduction process) to Pt.[56] In our synthesis of Au–Pd alloy nanodendrites, such shape-directing function originates probably from the binding interaction between DGA and Pd. This point will be discussed later.

Effect of Capping Agent. Different from the key role of ascorbic acid in inducing the formation of dendritic structure, the presence of capping agent was found to affect the size, shape, and uniformity of the NCs, instead of altering the nanodendrite structures. As shown in Figure 5a–d, when P123 was replaced by other capping agents such as Pluronic F127, Triton X-100, or PVP, nanodendrite structures were also formed, but their sizes and shapes are slightly different. For example, when Pluronic F127 was used as the capping agent, nanodendrites with ill-defined morphologies were obtained, but the size (~20 nm) was comparable to that in the case of P123 due to the similar structure of F127 to P123. However, when PVP was used as the capping agent, the sizes of nanodendrites became slightly larger, about 30 nm. It was interesting to find that when Triton X-100 was used as the capping agent, well-defined and globular-flower-like nanodendrites with sizes of 30–50 nm were yielded. Each flower was composed of tens to hundreds of small petals, suggesting its formation is a consequence of more advanced assembly. Moreover, similar flower-like NCs but composed of much denser assembly of petals were also formed even in the absence of any capping agent. Generally, the capping agent in the solution synthesis of NCs has two functions: one is to stabilize NCs against their aggregation, and the other is to direct the growth of NCs by preferential adsorption on specific crystal planes.[6−10,12,13] From the evolution tendency of the size and shape of nanodendrites with variation of the capping agent, we can propose that the function of the capping agent is to limit the assembly of primary petals to a suitable extent. Otherwise, they would aggregate into bigger and denser flower-like nanodendrites.

In terms of the size and uniformity of the nanodendrites as well as the accessibility of small branches in them to foreign molecules in the catalytic applications, we choose P123 as the most suitable capping agent. Subsequently, we investigated the effect of the concentration of P123 on the size and morphology of nanodendrites. As shown in Figure 5e,f, varying the P123 concentration in a wide range from 1.74 to 23.2 g/L did not result in appreciable changes in the size and morphology of nanodendrites, except for the slightly growing of primary branches in the case of 1.74 g/L. Therefore, in the other condition-optimizing experiments, we kept the concentration of P123 at 5.06 g/L.

Effect of Reduction Temperature. The reduction temperature usually affects the growth kinetics than the nucleation to a greater extent.[57] Figure 6 shows the TEM images of Au–Pd nanostructures synthesized at 0, 25, and 50

dx.doi.org/10.1021/jp4013202 | J. Phys. Chem. C 2013, 117, 12526–12536

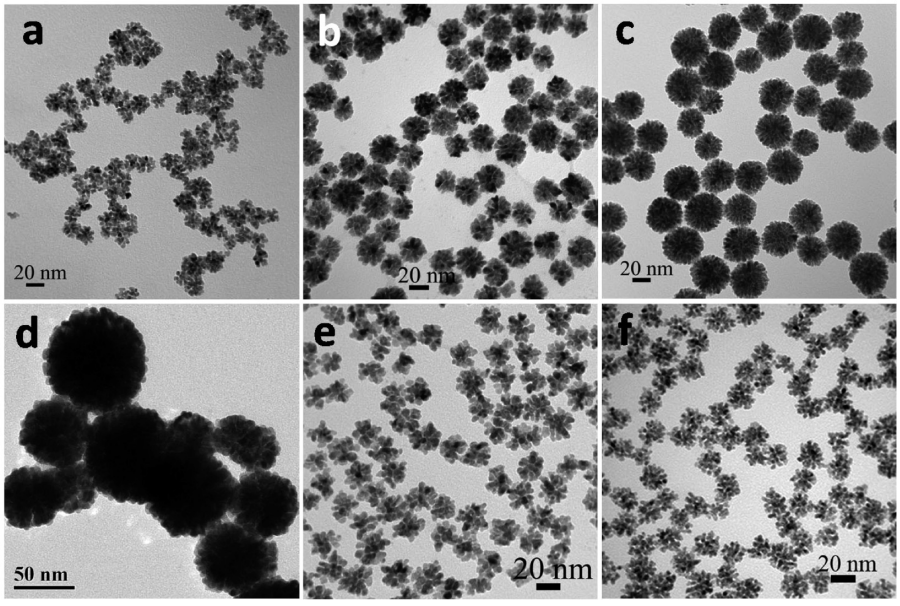

Figure 5. TEM images of Au−Pd nanostructures synthesized with different type and concentration of capping agent (a) 5.06 g/L Pluronic F127, (b) 5.06 g/L PVP, (c) 5.06 g/L Triton X-100, (d) in the absence of capping agent, (e) 1.74 g/L Pluronic P123, and (f) 23.2 g/L Pluronic P123.

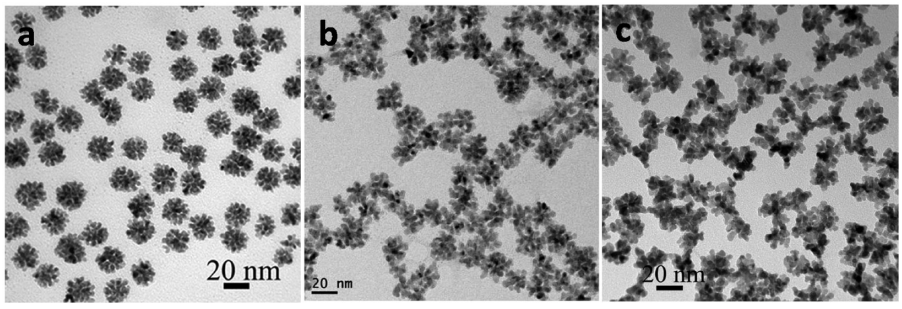

Figure 6. TEM images of Au−Pd nanostructures synthesized at different reaction temperatures: (a) 0, (b) 25, and (c) 50 °C.

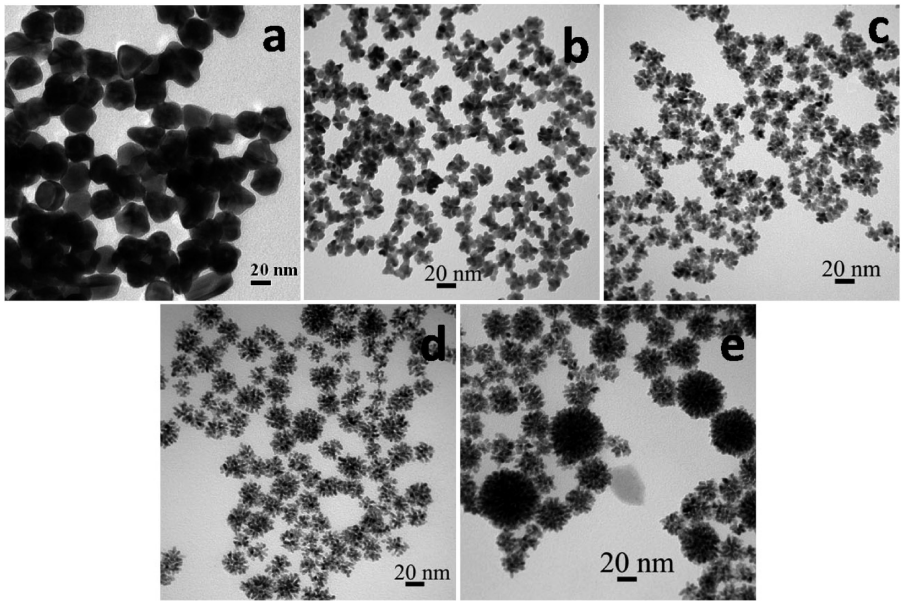

Figure 7. TEM images of Au−Pd nanostructures synthesized with different molar ratio of Au/Pd (a) 1/0, (b) 3/1, (c) 1/1, (d) 1/3, and (e) 0/1.

°C. It can be clearly seen that even when the reduction process occurred at as low as 0 °C, well-defined and uniform-sized nanodendrites were formed. However, when the reduction proceeded at a higher temperature, e.g., 50 °C, ill-defined

dx.doi.org/10.1021/jp4013202 | J. Phys. Chem. C 2013, 117, 12526−12536

nanodendrites with larger primary particles were produced, which was possibly caused by the overgrowth of particles. For the convenient operation, we choose 25 °C as the most suitable reduction temperature.

Effect of Au/Pd Ratio. One prominent advantage of bimetallic NCs over single metal counterparts lies in that the chemical composition is tunable in a wide range which will lead to the synergistic effect between the two components in catalytic applications.[18,22,29−34] Nevertheless, the changes in the atomic ratio of the two metals will also bring about, in some cases, the alteration of morphologies.[11,47,50,51] In the present work, we investigated the effect of Au/Pd atomic ratio on the structures of the NCs. For comparison, monometallic Au and Pd NCs were also synthesized at the same reaction conditions. As shown in Figure 7, in the absence of H_2PdCl_4 precursor, the reduction of $HAuCl_4$ with ascorbic acid produced nonuniform-sized and irregular-shaped gold NCs, and most of NCs were faceted, which is in agreement with reports in the literature.[58] For contrast, in the absence of $HAuCl_4$ precursor, hyperbranched nanodendrites of Pd with nonuniform size distribution (from 20 to 80 nm) were formed. This result is very similar to those Pt nanostructures produced by the reduction of ascorbic acid,[56] confirming the shape-directing function of ascorbic acid is accomplished via the binding interaction between DGA and Pd. For the Au−Pd bimetallic systems, well-defined and uniform-sized nanodendrites were obtained in a wide Au/Pd atomic ratio from 3/1 to 1/3. Furthermore, a higher content of Au was favorable to improve the uniformity of morphology and size of nanodendrites; meanwhile, it enlarged the crystal sizes of branches in the nanodendrites. On the contrary, a higher content of Pd gave smaller but a higher density of branches and a more scattering size distribution in the nanodendrites. The above results indicate that Pd plays an important role in the formation of nanodendrites while finely tuning the molar ratio of Au/Pd can produce well-defined and high-quality nanodendrites. This is reminiscent of our previous work on Au−Cu bimetallic NCs where the presence of Cu was also found to play a key role in inducing the nanowire network morphology.[11] Because of the different standard reduction potential of Au and Pd ions ($AuCl_4^-$/Au, 1.002 V, $PdCl_4^{2-}$/Pd, 0.591 V),[47] the variation in the Au/Pd atomic ratio will influence the nucleation process, which will in turn affect the primary metal particle sizes. Assisted by the shape-directing agent ascorbic acid, the branches will assemble into nanodendrites during the growth of NCs.

Table 1 lists the bulk and surface compositions of Au−Pd nanodendrites with different Au/Pd ratios, which were respectively determined by ICP and XPS. It can be clearly seen that the surface Au/Pd ratios are approximately the same as the bulk ones, indicating the homogeneous alloy rather than core@shell structure was formed under our synthesis conditions. This is distinguished from most of Au−Pd NCs reported earlier where enrichment of Pd on the surface was always observed.[45,47] The homogeneous alloy structure is resulted from the dropwise addition of metal precursors to the solution containing excess amount of ascorbic acid, which ensures coreduction of Au^{3+} and Pd^{2+} cations in spite of their different reduction potentials. This point will be further addressed in the following section.

Table 1. Bulk and Surface Au/Pd Ratios and the Binding Energies (BE) of Au−Pd Nanodendrites

sample	bulk Au/Pd ratio determined by ICP	surface Au/Pd ratio determined by XPS	BE(Pd $3d_{5/2}$) (eV)	BE(Au $4f_{7/2}$) (eV)
Au_3Pd_1	2.90/1	2.93/1	334.1	82.7
Au_1Pd_1	0.99/1	1.06/1	334.6	82.9
Au_1Pd_3	1/3.03	1/2.83	335.3	83.4
Pd			334.4	
Au				82.5

Evolution of Nanodendrites. It has been proposed that the formation of nanodendrites involves a slow nucleation and fast autocatalytic reduction aggregated process.[15,16,21−27] Moreover, in the presence of seeds, the formation of nanodendrites followed a seed-assisted growth mechanism, which concerned both homogeneous and heterogeneous nucleation of metal atoms and oriented attachment growth.[19] In the present work, to better understand the formation mechanism of Au−Pd nanodendrites, we investigated the morphology evolution of Au−Pd NCs by taking aliquots out of the reaction system at various dropping stage. Figure 8 shows the typical TEM images sampled at different dropping time. At the initial reaction stage (t = 80 s), a few faceted primary particles with sizes of 3−5 nm were produced (Figure 8a), and these primary particles had some tendency to aggregate via oriented attachment (Figure S2). To determine the phase composition of these primary particles formed at the very early stage of the reaction, we conducted HRTEM and XRD examinations. As shown in the inset of Figure 8a and Figure S2, the lattice distance of the particles is 2.30 Å which is well consistent with the (111) planes of Au−Pd alloy.[47] The EDS analysis of the individual particles also showed the presence of both Au and Pd (Figure S3). Moreover, the XRD patterns of the sample lie between those of Au and Pd (Figure S4). The phase composition, determined by using Vegard's law, is $Au_{0.6}Pd_{0.4}$, which is basically consistent with the chemical composition in the precursor as well as in the final nanodendrites. All these characterization results indicate that the Au−Pd alloy nanostructure has already formed at the very early time of the reaction. With continuous dropping addition of the reactant, more and more primary particles were formed, and some of them began to attach in an oriented way to form nanodendrites with few branches (Figure 8b,c). Moreover, it was noted that the sizes of branches were almost the same as the initially formed particles, suggesting that the dropping addition of the reactants at a constant flow rate does not induce the further growth of primary particles; instead, it can orient the attachment of primary particles for the formation of nanodendrites. At 23 min, all the precursors were dropped into the reaction system and well-defined nanodendrites were formed. Meanwhile, one could still observe a few primary particles (Figure 8f). With the further extension of reaction time to 1 h, all the nanoparticles assembled into nanodendrites. The UV−vis spectra of the samples taken from the reaction system at various dropping stages indicated that the Au−Pd alloy phase was always formed at different stages (Figure S5). From the above morphology evolution with the dropping addition time, we can propose that the formation of Au−Pd nanodendrites is the result of homogeneous nucleation followed by oriented attachment which is directed by the interaction between Pd and ascorbic acid-derived DGA. This is quite different from Au−Pd nanostructures synthesized by seed-mediated nucleation and growth where gold NC core is preformed and then followed by

dx.doi.org/10.1021/jp4013202 | J. Phys. Chem. C 2013, 117, 12526−12536

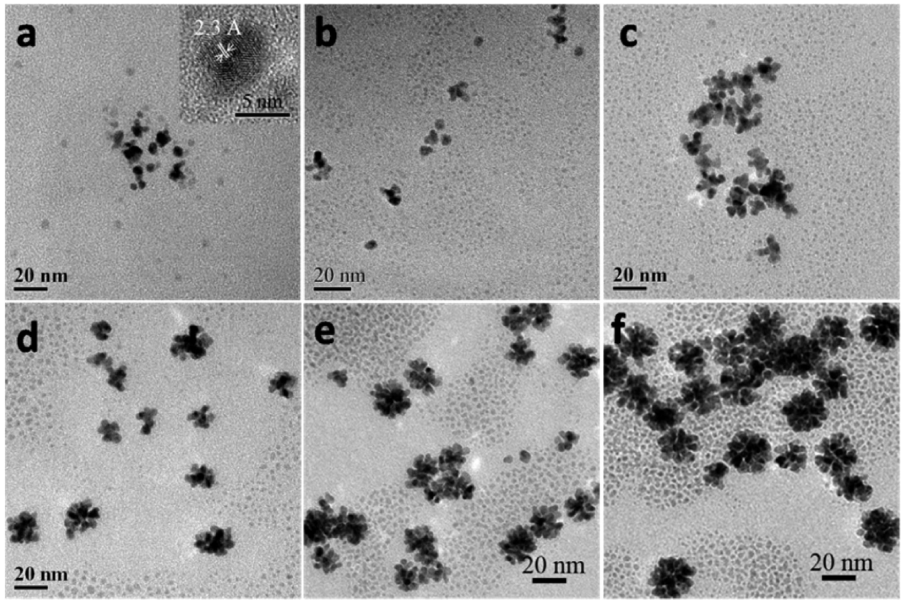

Figure 8. TEM images of Au−Pd nanostructures sampled at different dropping stage: (a) 80 s, (b) 140 s, (c) 4 min, (d) 8 min, (e) 15 min, and (f) 23 min. The inset is the HRTEM image of the sample at 80 s.

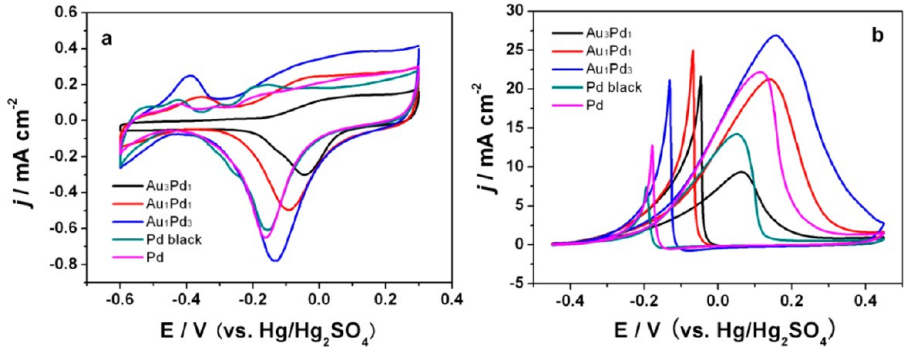

Figure 9. CVs of Au−Pd nanodendrites with different molar ratio Au/Pd and Pd black in (a) 0.1 M KOH at a scan rate of 20 mV s^{-1} and (b) 0.1 M KOH + 0.5 M methanol at a scan rate of 50 mV s^{-1}.

the reduction of Pd precursor[46] or coreduction of Au and Pd precursors.[50,51]

Electrocatalytic Activity for Methanol Oxidation. It has been reported that Pd-based NCs have a high electrocatalytic activity toward ethanol or methanol oxidation in alkaline solutions.[43−45,49] To evaluate the catalytic performance of the as-prepared Au−Pd alloy nanodendrites, the electrooxidation of methanol was performed. Figure 9a depicts the CV curves of Au−Pd nanodendrites with different atomic ratio of Au/Pd in N_2-saturated 0.1 M KOH solution at a scan rate of 20 mV s^{-1}. According to the literature,[49] the electrochemically active surface area (ECSA) of Pd can be obtained from the electric charges for oxygen desorption in PdO during the negative scan. The ECSA of the Au_1Pd_3, Au_1Pd_1, Au_3Pd_1, and Pd nanodendrites were measured to be 30.4, 19.0, 9.3, and 23.6 m^2 g^{-1}, respectively. Among Au−Pd alloy nanodendrites with various Au/Pd ratios, the ECSA decreased as an increase in the Au content, which can be attributed to the lower electrochemical activity of gold than palladium. However, it is interesting to find that the Au_1Pd_3 nanodendrite had a much larger ECSA than monometallic Pd nanodendrite, indicating a synergistic effect between Au and Pd. Commercial Pd black was also tested for comparison, and the ECSA for Pd black was 22.2 m^2 g^{-1}, which was slightly smaller than the Pd nanodendrite. Figure 9b displays the CVs of methanol oxidation in N_2-saturated aqueous solutions containing 0.1 M KOH and 0.5 M methanol. The current density was normalized by the geometric area of the electrode, as literature reported.[14] It can be observed that the peak current densities for Au_1Pd_3, Au_1Pd_1, Au_3Pd_1, and monometallic Pd nanodendrites in the positive scanning are 27.04, 21.42, 9.51, and 22.16 mA cm^{-2}, respectively, which agrees well with the trend of ECSA. Clearly, the Au_1Pd_3 nanodendrites exhibited the best electrocatalytic activity among various Au−Pd nanodendrites. Compared with commercial Pd black catalyst (14.36 mA cm^{-2}), the peak current density of Au_1Pd_3 was increased by 88%. The significant enhancement in the electrocatalytic activity of Au_1Pd_3 can be attributed to the improvement in the dendritic morphology on one hand. As shown in Figure 7, the crystal sizes of branches in the nanodendrites became smaller with an increase of the Pd content, and the diminished crystal sizes would be favorable to the enlargement of ECSA. On the other hand, the electronic property of Pd may also be modified by alloying with a small amount of Au. To support this point, we conducted XPS analysis of the samples with different Au/Pd ratio. As shown in Table 1 and Figure S6, the binding energy of Pd $3d_{5/2}$ in the

dx.doi.org/10.1021/jp4013202 | J. Phys. Chem. C 2013, 117, 12526−12536

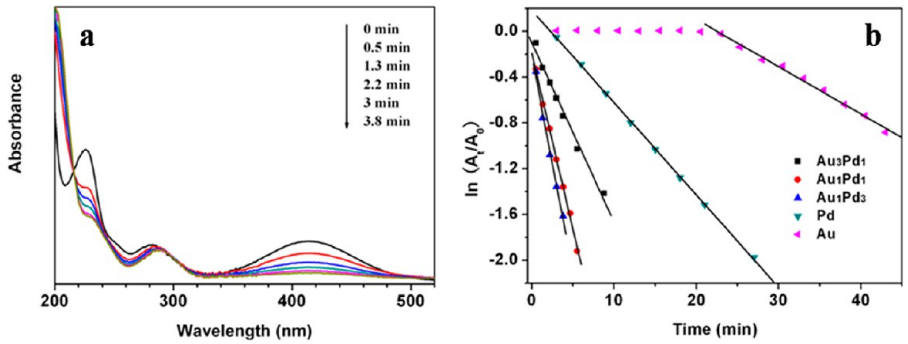

Figure 10. (a) Time-dependent UV−vis spectra of reaction solution catalyzed by Au/Pd = 1/3 nanodendrites. (b) Plots of $\ln(A_t/A_0)$ versus time for Au−Pd nanodendrites with different Au/Pd ratio.

monometallic Pd nanodendrites was 334.4 eV, which was 0.7 eV lower than metallic Pd (335.1 eV). Similarly, the binding energy of Au $4f_{7/2}$ in the monometallic Au NCs was 82.5 eV, which was 1.5 eV lower than metallic gold (84.0 eV). This result suggests that there is charge transfer from residual stabilizing agent Pluronic P123 to metal NCs, making them slightly negatively charged. In contrast, upon forming Au−Pd alloy, the binding energies of both Au and Pd shift toward higher values, making them more metallic. For example, the binding energies of Pd $3d_{5/2}$ and Au $4f_{7/2}$ in the Au_1Pd_3 nanodendrites were 335.3 and 83.4 eV, respectively, which were very close to metallic Pd and Au. Such a difference between Au−Pd alloy and monometallic counterparts can be tentatively attributed to the electronic modification of Pd by Au.[59] For the electro-oxidation of methanol, it was reported that the slightly positive shift of the d-band center of Pd could be favorable to the adsorption of methanol on Pd surface, which in turn enhanced the electrocatalytic activity.[60] Accordingly, the higher electrocatalytic activity of Au_1Pd_3 nanodendrites than monometallic Pd counterpart can be attributed both to the reduced size of primary crystals and to the modification of electronic property of Pd by alloying with gold.

Catalytic Reduction of 2-Nitrophenol. Au−Pd nanodendrites were also tested as catalysts for the reduction of 2-nitrophenol with $NaBH_4$.[61] The reaction was monitored by the change of UV−vis absorption spectra. In the absence of the catalyst, the absorption peak at 415 nm did not change with the reaction time, indicating the reduction reaction did not occur. However, in the presence of Au−Pd nanodendrites, the characteristic peak at 415 nm decreased in its intensity with the reaction time and disappeared completely at 3.8 min (Figure 10a), and concurrently, the solution became colorless, indicating the reduction of 2-nitrophenol into 2-aminophenol. Evidently, the Au−Pd nanodendrites were active for the reduction of 2-nitrophenol into 2-aminophenol. To compare the catalytic activities of Au−Pd nanodendrites with different Au/Pd ratios, we calculated the reaction rate constants by measuring the intensity (A) of absorption peak at 415 nm with the reaction time and plotting $\ln(A_t/A_0)$ versus reaction time t. As shown in Figure 10b, a linear relationship between $\ln(A_t/A_0)$ and reaction time t was obtained for all the catalysts, indicating the reaction is first-order with respect to 2-nitrophenol. This is reasonable considering the amount of $NaBH_4$ was greatly in excess. The rate constants (k), determined by the slopes of the lines, were 0.377, 0.308, 0.157, and 0.081 min^{-1} for Au_1Pd_3, Au_1Pd_1, Au_3Pd_1, and Pd nanodendrites, respectively. This result demonstrates a clear dependence of activity on the chemical composition of the nanodendrites; the Au−Pd alloy nanodendrites manifest a much higher activity than monometallic Pd counterpart, and their activities decrease with decreasing the Pd content in the bimetallic catalysts. In particular, the activity of Au_1Pd_3 nanodendrites is more than 4 times as high as that of pure Pd nanodendrites, showing a strong synergy between Au and Pd. It should be pointed out that monometallic gold NCs exhibited a rather poor activity due to the large crystal sizes (20−50 nm, in Figure 7a); no any reduction took place in the initial 25 min. Since both Au and Pd monometallic NCs were poorly active, the superior activities of Au−Pd alloy nanodendrites could be attributed to the synergy between Au and Pd, and this synergy could be understood in terms of decreased crystal sizes and electronic modifications, as we discussed in the electro-oxidation of methanol. Finally, we would like to stress that our best catalyst Au_1Pd_3 is 8-fold more active than that reported in literature in terms of activity per mass of catalyst (Table S1),[61] showing great potentials in catalytic applications.

CONCLUSIONS

In summary, we have developed a facile and reproducible method for the synthesis of Au−Pd bimetallic nanodendrites with homogeneous alloy structure and well-defined morphology, by using ascorbic acid as the reducing agent and P123 as the capping agent. The dropping addition of the metal precursors solution to the ascorbic solution in the presence of P123 enables simultaneous coreduction of Au and Pd meanwhile controls well the uniform primary particle sizes. The formation of the nanodendrites is a result of homogeneous nucleation followed by oriented attachment of primary particles. Ascorbic acid plays a key role in directing the attachment of primary particles toward a dendritic morphology, through its binding interaction to Pd. The resultant Au−Pd nanodendrites exhibited excellent catalytic activities toward methanol oxidation and reduction of 2-nitrophenol, and the catalytic performances could be effectively tuned by varying the molar ratio of Au/Pd.

ASSOCIATED CONTENT

Supporting Information

Scheme of the synthesis procedure, the TEM images, XRD patterns, UV−vis spectra, XPS spectra of the Au−Pd nanodendrites, and the activity per mass of catalyst for the reduction of 2-nitrophenol over Au−Pd nanodendrites. This material is available free of charge via the Internet at http://pubs.acs.org.

AUTHOR INFORMATION

Corresponding Author

*Tel +86 411 84379015; Fax +86 411 84691570; e-mail taozhang@dicp.ac.cn (T.Z.).

Notes

The authors declare no competing financial interest.

ACKNOWLEDGMENTS

Support from the National Natural Science Foundation of China (NSFC 20773124, 21176235, and 21103173) is gratefully acknowledged.

REFERENCES

(1) Haruta, M. Size- and Support-Dependency in the Catalysis of Gold. *Catal. Today* **1997**, *36*, 153−166.

(2) Haruta, M. When Gold Is Not Noble: Catalysis by Nanoparticles. *Chem. Rec.* **2003**, *3*, 75−87.

(3) Chen, M. S.; Goodman, D. W. The Structure of Catalytically Active Gold on Titania. *Science* **2004**, *306*, 252−255.

(4) Qiao, B. T.; Wang, A. Q.; Yang, X. F.; Allard, L. F.; Jiang, Z.; Cui, Y. T.; Liu, J. Y.; Li, J.; Zhang, T. Single-Atom Catalysis of CO Oxidation Using Pt_1/FeO_x. *Nat. Chem.* **2011**, *3*, 634−641.

(5) Lin, J.; Qiao, B. T.; Liu, J. Y.; Huang, Y. Q.; Wang, A. Q.; Li, L.; Zhang, W. S.; Allard, L. F.; Wang, X. D.; Zhang, T. Design of a Highly Active Ir/$Fe(OH)_x$ Catalyst: Versatile Application of Pt-Group Metals for the Preferential Oxidation of Carbon Monoxide. *Angew. Chem., Int. Ed.* **2012**, *51*, 2920−2924.

(6) Sun, Y. G.; Xia, Y. N. Shape-Controlled Synthesis of Gold and Silver Nanoparticles. *Science* **2002**, *298*, 2176−2179.

(7) Tian, N.; Zhou, Z. Y.; Sun, S. G.; Ding, Y.; Wang, Z. L. Synthesis of Tetrahexahedral Platinum Nanocrystals with High-index Facets and High Electro-Oxidation Activity. *Science* **2007**, *316*, 732−735.

(8) Crespo-Quesada, M.; Yarulin, A.; Jin, M. S.; Xia, Y. N.; Kiwi-Minsker, L. Structure Sensitivity of Alkynol Hydrogenation on Shape- and Size-Controlled Palladium Nanocrystals: Which Sites Are Most Active and Selective? *J. Am. Chem. Soc.* **2011**, *133*, 12787−12794.

(9) Niu, W. X.; Zhang, L.; Xu, G. B. Shape-Controlled Synthesis of Single-Crystalline Palladium Nanocrystals. *ACS Nano* **2010**, *4*, 1987−1996.

(10) Yuan, Q.; Zhuang, J.; Wang, X. Single-Phase Aqueous Approach toward Pd Sub-10 nm Nanocubes and Pd-Pt Heterostructured Ultrathin Nanowires. *Chem. Commun.* **2009**, 6613−6615.

(11) Shi, L. H.; Wang, A. Q.; Huang, Y. Q.; Chen, X. W.; Delgado, J. J.; Zhang, T. Facile Synthesis of Ultrathin AuCu Dimetallic Nanowire Networks. *Eur. J. Inorg. Chem.* **2012**, *2012*, 2700−2706.

(12) Yin, A. X.; Min, X. Q.; Zhang, Y. W.; Yan, C. H. Shape-Selective Synthesis and Facet-Dependent Enhanced Electrocatalytic Activity and Durability of Monodisperse Sub-10 nm Pt-Pd Tetrahedrons and Cubes. *J. Am. Chem. Soc.* **2011**, *133*, 3816−3819.

(13) Niu, Z. Q.; Peng, Q.; Gong, M.; Rong, H. P.; Li, Y. D. Oleylamine-Mediated Shape Evolution of Palladium Nanocrystals. *Angew. Chem., Int. Ed.* **2011**, *50*, 6315−6319.

(14) Yin, J.; Wang, J. H.; Zhang, Y. J.; Li, H. Q.; Song, Y. J.; Jin, C. Z.; Lu, T.; Zhang, T. Monomorphic Platinum Octapod and Tripod Nanocrystals Synthesized by an Iron Nitrate Modified Polyol Process. *Chem. Commun.* **2011**, *47*, 11966−11968.

(15) Wang, L.; Guo, S. J.; Zhai, J. F.; Dong, S. J. Facile Synthesis of Platinum Nanoelectrocatalyst with Urchinlike Morphology. *J. Phys. Chem. C* **2008**, *112*, 13372−13377.

(16) Teng, X. W.; Liang, X. Y.; Maksimuk, S.; Yang, H. Synthesis of Porous Platinum Nanoparticles. *Small* **2006**, *2*, 249−253.

(17) Mohanty, A.; Garg, N.; Jin, R. C. A Universal Approach to the Synthesis of Noble Metal Nanodendrites and Their Catalytic Properties. *Angew. Chem., Int. Ed.* **2010**, *49*, 4962−4966.

(18) Lim, B.; Jiang, M. J.; Camargo, P. H. C.; Cho, E. C.; Tao, J.; Lu, X. M.; Zhu, Y. M.; Xia, Y. N. Pd-Pt Bimetallic Nanodendrites with High Activity for Oxygen Reduction. *Science* **2009**, *324*, 1302−1305.

(19) Lim, B.; Jiang, M. J.; Yu, T.; Camargo, P. H. C.; Xia, Y. N. Nucleation and Growth Mechanisms for Pd-Pt Bimetallic Nanodendrites and Their Electrocatalytic Properties. *Nano Res.* **2010**, *3*, 69−80.

(20) Peng, Z. M.; Yang, H. Synthesis and Oxygen Reduction Electrocatalytic Property of Pt-on-Pd Bimetallic Heteronanostructures. *J. Am. Chem. Soc.* **2009**, *131*, 7542−7543.

(21) Ataee-Esfahani, H.; Wang, L.; Nemoto, Y.; Yamauchi, Y. Synthesis of Bimetallic Au@Pt Nanoparticles with Au Core and Nanostructured Pt Shell toward Highly Active Electrocatalysts. *Chem. Mater.* **2010**, *22*, 6310−6318.

(22) Wang, L.; Nemoto, Y.; Yamauchi, Y. Direct Synthesis of Spatially-Controlled Pt-on-Pd Bimetallic Nanodendrites with Superior Electrocatalytic Activity. *J. Am. Chem. Soc.* **2011**, *133*, 9674−9677.

(23) Wang, L.; Yamauchi, Y. Strategic Synthesis of Trimetallic Au@Pd@Pt Core−Shell Nanoparticles from Poly(vinylpyrrolidone)-Based Aqueous Solution toward Highly Active Electrocatalysts. *Chem. Mater.* **2011**, *23*, 2457−2465.

(24) Song, Y. J.; Yang, Y.; Medforth, C. J.; Pereira, E.; Singh, A. K.; Xu, H. F.; Jiang, Y. B.; Brinker, C. J.; van Swol, F.; Shelnutt, J. A. Controlled Synthesis of 2-D and 3-D Dendritic Platinum Nanostructures. *J. Am. Chem. Soc.* **2004**, *126*, 635−645.

(25) Wang, L.; Yamauchi, Y. Block Copolymer Mediated Synthesis of Dendritic Platinum Nanoparticles. *J. Am. Chem. Soc.* **2009**, *131*, 9152−9153.

(26) Wang, L.; Yamauchi, Y. Autoprogrammed Synthesis of Triple-Layered Au@Pd@Pt Core-Shell Nanoparticles Consisting of a Au@Pd Bimetallic Core and Nanoporous Pt Shell. *J. Am. Chem. Soc.* **2010**, *132*, 13636−13638.

(27) Wang, Y. L.; Camargo, P. H. C.; Skrabalak, S. E.; Gu, H. C.; Xia, Y. N. A Facile, Water-Based Synthesis of Highly Branched Nanostructures of Silver. *Langmuir* **2008**, *24*, 12042−12046.

(28) Yin, J.; Wang, J. H.; Li, M. R.; Jin, C. Z.; Zhang, T. Iodine Ions Mediated Formation of Monomorphic Single-Crystalline Platinum Nanoflowers. *Chem. Mater.* **2012**, *24*, 2645−2654.

(29) Wang, A. Q.; Liu, J. H.; Lin, S. D.; Lin, T. S.; Mou, C. Y. A Novel Efficient Au-Ag Alloy Catalyst System: Preparation, Activity, and Characterization. *J. Catal.* **2005**, *233*, 186−197.

(30) Wang, A. Q.; Chang, C. M.; Mou, C. Y. Evolution of Catalytic Activity of Au-Ag Bimetallic Nanoparticles on Mesoporous Support for CO Oxidation. *J. Phys. Chem. B* **2005**, *109*, 18860−18867.

(31) Liu, X. Y.; Wang, A. Q.; Wang, X. D.; Mou, C. Y.; Zhang, T. Au-Cu Alloy Nanoparticles Confined in SBA-15 as a Highly Efficient Catalyst for CO Oxidation. *Chem. Commun.* **2008**, *28*, 3187−3189.

(32) Liu, X. Y.; Wang, A. Q.; Yang, X. F.; Zhang, T.; Mou, C. Y.; Su, D. S.; Li, J. Synthesis of Thermally Stable and Highly Active Bimetallic Au-Ag Nanoparticles on Inert Supports. *Chem. Mater.* **2009**, *21*, 410−418.

(33) Liu, X. Y.; Wang, A. Q.; Zhang, T.; Su, D. S.; Mou, C. Y. Au-Cu Alloy Nanoparticles Supported on Silica Gel as Catalyst for CO Oxidation: Effects of Au/Cu Ratios. *Catal. Today* **2011**, *160*, 103−108.

(34) Liu, X. Y.; Wang, A. Q.; Li, L.; Zhang, T.; Mou, C. Y.; Lee, J. F. Structural Changes of Au-Cu Bimetallic Catalysts in CO Oxidation: In situ XRD, EPR, XANES, and FT-IR Characterizations. *J. Catal.* **2011**, *278*, 288−296.

(35) Enache, D. I.; Edwards, J. K.; Landon, P.; Solsona, B. E.; Carley, A. F.; Herzing, A. A.; Watanabe, M.; Kiely, C. J.; Knight, D. W.; Hutchings, G. J. Solvent-Free Oxidation of Primary Alcohols to Aldehydes Using Au-Pd/TiO_2 Catalysts. *Science* **2006**, *311*, 362−365.

(36) Marx, S.; Baiker, A. Beneficial Interaction of Gold and Palladium in Bimetallic Catalysts for the Selective Oxidation of Benzyl Alcohol. *J. Phys. Chem. C* **2009**, *113*, 6191−6201.

(37) Miedziak, P. J.; Tang, Z.; Davies, T. E.; Enache, D. I.; Bartley, J. K.; Carley, A. F.; Herzing, A. A.; Kiely, C. J.; Taylor, S. H.; Hutchings, G. J. Ceria Prepared Using Supercritical Antisolvent Precipitation: a Green Support for Gold-Palladium Nanoparticles for the Selective Catalytic Oxidation of Alcohols. *J. Mater. Chem.* **2009**, *19*, 8619−8627.

(38) Wang, D.; Villa, A.; Porta, F.; Prati, L.; Su, D. S. Bimetallic Gold/Palladium Catalysts: Correlation between Nanostructure and Synergistic Effects. *J. Phys. Chem. C* **2008**, *112*, 8617−8622.
(39) Edwards, J. K.; Solsona, B. E.; Landon, P.; Carley, A. F.; Herzing, A.; Kiely, C. J.; Hutchings, G. J. Direct Synthesis of Hydrogen Peroxide from H_2 and O_2 Using TiO_2-Supported Au-Pd Catalysts. *J. Catal.* **2005**, *236*, 69−79.
(40) Edwards, J. K.; Thomas, A.; Carley, A. F.; Herzing, A. A.; Kiely, C. J.; Hutchings, G. J. Au-Pd Supported Nanocrystals as Catalysts for the Direct Synthesis of Hydrogen Peroxide from H_2 and O_2. *Green Chem.* **2008**, *10*, 388−394.
(41) Edwards, J. K.; Pritchard, J.; Piccinini, M.; Shaw, G.; He, Q.; Carley, A. F.; Kiely, C. J.; Hutchings, G. J. The Effect of Heat Treatment on the Performance and Structure of Carbon-Supported Au-Pd Catalysts for the Direct Synthesis of Hydrogen Peroxide. *J. Catal.* **2012**, *292*, 227−238.
(42) Wei, X.; Yang, X. F.; Wang, A. Q.; Li, L.; Liu, X. Y.; Zhang, T.; Mou, C. Y.; Li, J. Bimetallic Au-Pd Alloy Catalysts for N_2O Decomposition: Effects of Surface Structures on Catalytic Activity. *J. Phys. Chem. C* **2012**, *116*, 6222−6232.
(43) Song, H. M.; Moosa, B. A.; Khashab, N. M. Water-Dispersable Hybrid Au-Pd Nanoparticles as Catalysts in Ethanol Oxidation, Aqueous Phase Suzuki-Miyaura and Heck Reactions. *J. Mater. Chem.* **2012**, *22*, 15953−15959.
(44) Lu, C. L.; Prasad, K. S.; Wu, H. L.; Ho, J. A.; Huang, M. H. Au Nanocube-Directed Fabrication of Au-Pd Core-Shell Nanocrystals with Tetrahexahedral, Concave Octahedral, and Octahedral Structures and Their Electrocatalytic Activity. *J. Am. Chem. Soc.* **2010**, *132*, 14546−14553.
(45) Hong, J. W.; Lee, Y. W.; Kim, M.; Kang, S. W.; Han, S. W. One-Pot Synthesis and Electrocatalytic Activity of Octapodal Au-Pd Nanoparticles. *Chem. Commun.* **2011**, *47*, 2553−2555.
(46) Xu, J.; Wilson, A. R.; Rathmell, A. R.; Howe, J.; Chi, M.; Wiley, B. J. Synthesis and Catalytic Properties of Au-Pd Nanoflowers. *ACS Nano* **2011**, *5*, 6119−6127.
(47) Han, J. S.; Zhou, Z. W.; Yin, Y.; Luo, X. T.; Li, J.; Zhang, H.; Yang, B. One-Pot, Seedless Synthesis of Flowerlike Au-Pd Bimetallic Nanoparticles with Core-Shell-like Structure via Sodium Citrate Coreduction of Metal Ions. *CrystEngComm* **2012**, *14*, 7036−7042.
(48) Lee, Y. W.; Kim, N. H.; Lee, K. Y.; Kwon, K.; Kim, M.; Han, S. W. Synthesis and Characterization of Flower-Shaped Porous Au-Pd Alloy Nanoparticles. *J. Phys. Chem. C* **2008**, *112*, 6717−6722.
(49) Lee, Y. W.; Kim, M.; Kim, Y.; Kang, S. W.; Lee, J. H.; Han, S. W. Synthesis and Electrocatalytic Activity of Au-Pd Alloy Nanodendrites for Ethanol Oxidation. *J. Phys. Chem. C* **2010**, *114*, 7689−7693.
(50) DeSantis, C. J.; Peverly, A. A.; Peters, D. G.; Skrabalak, S. E. Octopods versus Concave Nanocrystals: Control of Morphology by Manipulating the Kinetics of Seeded Growth via Co-Reduction. *Nano Lett.* **2011**, *11*, 2164−2168.
(51) DeSantis, C. J.; Sue, A. C.; Bower, M. M.; Skrabalak, S. E. Seed-Mediated Co-reduction: A Versatile Route to Architecturally Controlled Bimetallic Nanostructures. *ACS Nano* **2012**, *6*, 2617−2628.
(52) Boudeville, Y.; Figueras, F.; Forissier, M.; Portefaix, J.; Vedrine, J. C. Correlations between X-ray Photoelectron Spectroscopy Data and Catalytic Properties in Selective Oxidation on Sb-Sn-O Catalysts. *J. Catal.* **1979**, *58*, 52−60.
(53) Scofield, J. H. Hartree-Slater Subshell Photoionization Cross-Sections at 1254 and 1487 eV. *J. Electron Spectrosc. Relat. Phenom.* **1976**, *8*, 129−137.
(54) Zhang, H.; Li, W. Y.; Jin, M. S.; Zeng, J.; Yu, T.; Yang, D. R.; Xia, Y. N. Controlling the Morphology of Rhodium Nanocrystals by Manipulating the Growth Kinetics with a Syringe Pump. *Nano Lett.* **2011**, *11*, 898−903.
(55) Zeng, J.; Zhu, C.; Tao, J.; Jin, M. S.; Zhang, H.; Li, Z. Y.; Zhu, Y. M.; Xia, Y. N. Controlling the Nucleation and Growth of Silver on Palladium Nanocubes by Manipulating the Reaction Kinetics. *Angew. Chem., Int. Ed.* **2012**, *51*, 2354−2358.
(56) Wang, L.; Hu, C. P.; Nemoto, Y.; Tateyama, Y.; Yamauchi, Y. On the Role of Ascorbic Acid in the Synthesis of Single-Crystal Hyperbranched Platinum Nanostructures. *Cryst. Growth Des.* **2010**, *10*, 3454−3460.
(57) Zhu, C.; Zeng, J.; Tao, J.; Johnson, M. C.; Schmidt-Krey, I.; Blubaugh, L.; Zhu, Y. M.; Gu, Z. Z.; Xia, Y. N. Kinetically Controlled Overgrowth of Ag or Au on Pd Nanocrystal Seeds: From Hybrid Dimers to Nonconcentric and Concentric Bimetallic Nanocrystals. *J. Am. Chem. Soc.* **2012**, *134*, 15822−15831.
(58) Sau, T. K.; Murphy, C. J. Room Temperature, High-Yield Synthesis of Multiple Shapes of Gold Nanoparticles in Aqueous Solution. *J. Am. Chem. Soc.* **2004**, *126*, 8648−8649.
(59) Murugadoss, A.; Okumura, K.; Sakurai, H. Bimetallic AuPd Nanocluster Catalysts with Controlled Atomic Gold Distribution for Oxidative Dehydrogenation of Tetralin. *J. Phys. Chem. C* **2012**, *116*, 26776−26783.
(60) Tan, Q.; Du, C. Y.; Yin, G. P.; Zuo, P. J.; Cheng, X. Q.; Chen, M. Highly Efficient and Stable Nonplatinum Anode Catalyst with Au@Pd Core-Shell Nanostructures for Methanol Electrooxidation. *J. Catal.* **2012**, *295*, 217−222.
(61) Liu, H. Y.; Yang, Q. Facile Fabrication of Nanoporous Au-Pd Bimetallic Foams with High Catalytic Activity for 2-Nitrophenol Reduction and SERS Property. *J. Mater. Chem.* **2011**, *21*, 11961−11967.